

Multi-Layer Confidence Scoring for Detection of Out-of-Distribution Samples, Adversarial Attacks, and In-Distribution Misclassifications

Lorenzo Capelli*, Leandro de Souza Rosa*, Gianluca Setti^{††}, Mauro Mangia^{*†}, Riccardo Rovatti^{*†}

^{*}DEI, [†]ARCES, University of Bologna, Italy, [‡]CEMSE, KAUST, Saudi Arabia

{l.capelli, leandro.desouzarosa, mauro.mangia, riccardo.rovatti}@unibo.it, gianluca.setti@kaust.edu.sa

Abstract—The recent explosive growth in Deep Neural Networks applications raises concerns about the black-box usage of such models, with limited transparency and trustworthiness in high-stakes domains, which have been crystallized as regulatory requirements such as the European Union Artificial Intelligence Act. While models with embedded confidence metrics have been proposed, such approaches cannot be applied to already existing models without retraining, limiting their broad application. On the other hand, post-hoc methods, which evaluate pre-trained models, focus on solving problems related to improving the confidence in the model’s predictions, and detecting Out-Of-Distribution or Adversarial Attacks samples as independent applications. To tackle the limited applicability of already existing methods, we introduce Multi-layer Analysis for Confidence Scoring (MACS), a unified post-hoc framework that analyzes intermediate activations to produce classification-maps. From the classification-maps, we derive a score applicable for confidence estimation, detecting distributional shifts and adversarial attacks, unifying the three problems in a common framework, and achieving performances that surpass the state-of-the-art approaches in our experiments with the VGG16 and ViTb16 models with a fraction of their computational overhead.

Index Terms—Trustworthiness, Deep Neural Networks, Intermediate Activations, Decision Process Analysis

I. INTRODUCTION

Over the past decade, Artificial Intelligence (AI) has attracted substantial attention, especially due to the performances reached by Deep Neural Networks (DNNs) across many domains. Typically, DNNs are used as black-box systems, making it challenging to understand how specific inputs lead to particular outputs and impossible to trace the origin of an error. Furthermore, the lack of understanding limits both critical trustworthiness and transparency in DNNs, both important requirements for high-risk domains such as healthcare, finance, and autonomous systems. These concepts have been recently crystallized as the European Union (EU)’s AI Act [1], which categorizes systems affecting critical domains as high-risk and mandates transparency, explainability, and human oversight.

To enhance trust in human-AI interaction, there is a growing need for DNNs certification tools for addressing issues such as confidence estimation, i.e., determining whether In-Distribution (ID) samples are correctly classified by the DNN [2], [3], and Out-Of-Distribution (OOD) and Adversarial Attack (AA) detection [4]. While these issues are often studied

separately in the literature, classification reliability is compromised in all three cases, and their shared underlying nature suggests the need for a unified detection framework. However, current methods for confidence estimation often fail when applied to OOD or AA scenarios, and similarly, techniques designed for OOD or AA detection have never been explored for confidence estimation.

Methods to tackle these problems are traditionally divided into two families: ante-hoc, which focus on developing new DNN models emphasizing trustworthiness; and post-hoc methods that extract information from existing models, being more broadly applicable, and hence the focus of this paper.

Moreover, recent research goes beyond analyzing only the model’s outputs, focusing on complementing DNNs’ prediction with intermediate activations analysis to enhance trustworthiness [5], [4]. Nevertheless, such methods are often limited to small models due to the activations’ high dimensionality.

This paper introduces Multi-layer Analysis for Confidence Scoring (MACS), a framework for analyzing the intermediate activations produced by a pre-trained DNN using classical signal-processing techniques, including a dimensionality reduction step to ensure scalability, an unsupervised clustering to associate activation space-level features with human-interpretable ones. MACS returns a confidence metric that quantifies the reliability of a DNN’s internal decision-making process. The proposed methodology imposes no limitations on either the number of layers processed in parallel or the types of layers it can handle. MACS’s architecture aligns with the EU’s AI Act’s requirements by providing an audit-friendly and unified multi-layer evaluation applicable to confidence estimation, OOD, and AA detection, further enhancing deployability in real-world systems constrained by regulatory or safety concerns.

The rest of this paper is organized as follows: Section II presents the related work. Section III formally defines the proposed framework. Section IV describes the applications, models, and datasets used for testing. Section V presents results when applying the proposed framework for confidence estimation, and OOD and AA detection. Finally, Section VI concludes the paper.

II. RELATED WORKS

As the EU’s AI Act’s requirements reflect on improving DNNs’ robustness and trustworthiness, a vast amount of recent

research focuses on confidence estimation, and OOD and AA detection. Below, we position our work relative to State-Of-The-Art (SOTA) approaches across several relevant axes.

A. Confidence Estimation and Trustworthiness

As DNNs typically provide predictions regardless of their input, a confidence estimate capturing the reliability of the prediction is a direct way to improve the model's trustworthiness.

Historically, softmax-based confidence measures MSP [6] have been adopted, in the case of neural classifiers, since its output intrinsically encodes the probabilities of a sample belonging to the available classes. However, it has been shown that, for modern DNNs such outputs are poorly calibrated, especially convolution-based ones [7], necessitating specific training procedures, ante-hoc methods, or the post-hoc computation of calibration functions [8], [9]. Nevertheless, calibration-based approaches may create undesirable shifts in the distribution of correctly- and miss-classified samples [10], prejudice already calibrated classifiers [11], and degrade under data scarcity [12], defeating the purpose of providing a reliable confidence score and leading recent research to focus on ante-hoc methods to solve these issues [11], [13].

Opposing calibration, recent research focuses on using uncertainty estimates as a proxy for a confidence score. Despite the mathematical soundness and application success of Bayesian estimators [14], their prohibitive computational costs have led to the development of dropout-based training methods, resulting in DNNs with embedded uncertainty estimation [15], which is implicitly and explicitly regularized [16]. Other ante-hoc methods focus on appending a Gaussian Process (GP) step to capture the epistemic uncertainty of data [17], without which the capability of predicting OOD samples is reduced [18], or a classifier [19], used to fine-tune the DNN to OOD detection.

On the other hand, post-hoc epistemic uncertainty estimation methods are an alternative to capturing relationships between data, acting similarly to calibration, as they fit a confidence estimate function based on the model's predictions over a training set. An early approach to use a decision risk as a confidence estimation [20], which has been recently extended by Detecting Out-of-distribution and misclassifications by Confident score calibration (DOC) [2], and Relative Uncertainty (Rel-U) [3] through considering the distributions of correctly- and miss-classified samples by the model, creating a confidence estimate based on the Kullback–Leibler (KL) divergence, or on a relative epistemic uncertainty, respectively. DOC and Rel-U are considered the SOTA on confidence estimation based on the model's output, outperforming calibration methods and other approaches in the same family.

Opposing uncertainty-based methods, MACS is a post-hoc method that approaches confidence estimation from the intermediate activation analysis side, capturing intra-data dependencies in a feature association step.

B. Intermediate Activation Analysis

To analyze the model's decision process, recent research focuses on evaluating the model's intermediate activations.

A first example is Deep k-Nearest Neighbors (DkNN) [5], which applies a k Nearest Neighbors (k-NN) on the activations extracted from different layers, yielding clusters of samples that enable a confidence score estimation based on the number of neighbors agreeing with the prediction, applicable to both OOD and AA detection.

Focusing on Convolutional Neural Networks (CNNs), Deep Mahalanobis Detector (DMD) [4] proposes computing a confidence score based on perturbations of a dimensionality-reduced representation of the intermediate activations, and training a regressor to detect OOD or AA samples. Nevertheless, DMD's shortcomings are its restriction to convolutional layers and the necessity of OOD/AA samples to fit its regressor. Most recently, [21] proposes an AA detection method that estimates a confidence score by comparing intermediate activations against Coverage Analysis Method (CAM)-based signatures derived from typical activation values for samples in a reference dataset. [22] proposes clustering the intermediate activations and performing an association step, leveraging empirical relationships between Low-Level Features (LLFs) within the DNN's activation and High-Level Features (HLFs) perceived by humans.

We highlight that analyzing intermediate activations directly is not a scalable approach, as modern DNNs easily reach dimensionalities over 1M, being detrimental for distance-based methods such as clustering. To address this limitation, MACS uses a Singular Value Decomposition (SVD) dimensionality reduction step, which we show applies to both linear and convolutional, allowing leveraging the association between LLFs and HLFs from [22].

C. Adversarial Attack Detection

As AAs are subtle modifications that lead the model to provide an incorrect prediction without altering the input's semantic meaning to the human user, they pose a reliability threat to systems deployed in practical and safety-critical applications.

In image classification tasks, AAs are generated by applying small perturbations to the input image. As such, approaches for AAs detection often rely on filtering to generate multiple samples, performing detection based on the model's outputs to these samples. One of the most well-established approaches in this family is Feature Squeezing (FS) [23], which applies multiple filters on the input and compares the model's decision on the computed variants against the original one to identify the presence of an AA. Similarly, [24] applies a smoothing filter based on the sample's entropy, and differently, [25] creates variants through perturbations. The main limitations of these methods are that they are applicable only to image classifiers, and attacks can be devised to avoid detection [26].

Regarding intermediate activations analysis, early approaches on AAs propose creating a complementary classifier fitted with normal and attacked samples on the intermediate activations [27]. Furthermore, the previously mentioned DkNN [5] and DMD [4] also apply in this scenario.

MACS enables efficient adversarial detection by comparing the model's decision process against expected values for the attacked prediction.

D. Reference Approaches

In this section, we position our method relative to the reference approaches. Because it leverages intermediate activation analysis, MACS can address confidence estimation, OOD detection, and AA detection within a unified scheme, offering greater flexibility than existing methods.

MSP: As the model itself is its best estimator, its outputs are typically the most efficient metric for confidence estimation. This makes MSP [6] a strong baseline for misclassifications detection, which is computed as the maximum value of the model’s output after a softmax normalization.

DOC: DOC [2] is a post-hoc method for confidence estimation and OOD detection. It computes a score based on the Gini’s impurity of the model’s softmax output and has two tunable hyper-parameters: temperature scaling and magnitude. The former sharpens the model’s output based on its distribution over a validation set. When the magnitude is set to a positive value, the method applies a gradient-based input perturbation, similar to an adversarial processing step, highlighting features that influence the model’s confidence.

Relative Uncertainty: Rel-U [3] introduces a data-driven measure of relative uncertainty for confidence estimation and OOD detection. It learns a class-wise distance matrix from correctly and incorrectly classified samples over a validation set, assigning higher uncertainty to misclassified instances. The resulting score is computed in closed form from the softmax outputs, after a temperature scaling step, which needs to be tuned. Similar to DOC, Rel-U employs an input pre-processing step controlled by a magnitude hyper-parameter, which back-propagates the learned metric to enhance separability. Through a third hyperparameter, the proposed method balances the trade-off between minimizing uncertainty for correctly classified samples and maximizing it for misclassified ones.

Deep Mahalanobis Detector: DMD [4] models the intermediate activations of CNNs distribution for detecting OOD and AA samples. The authors introduce a simplified variant, which we referred to as DMD base (DMD-b), and which analyzes the statistical distribution of pre-logits activations. As proposed in the previous approaches, back-propagation is applied to create a variation of the original sample based on the minimum Mahalanobis distance of the pre-logits activation with respect to each class training distribution. The framework is subsequently extended to a multi-layer formulation by applying the same analysis to convolutional layers after reducing them via average pooling. The evaluation of all layers’ scores is done empirically, by training a logistic regressor on the scores extracted from each layer to differentiate the vector of scores over a positive dataset ($\mathcal{D}_{\text{DMD}}^+$), usually the ID validation set, and a negative one ($\mathcal{D}_{\text{DMD}}^-$), typically OOD or AA validation samples.

The multi-layer version can be set in two modes: DMD aware (DMD-a) is set by using samples from the same dataset it is tested on as $\mathcal{D}_{\text{DMD}}^-$, hence being a supervised method with expected high-performance, which we interpret as an upper-bound; DMD unaware (DMD-u) is set by using samples from a dataset different than the one it is tested on as $\mathcal{D}_{\text{DMD}}^-$, hence being a realistic case in which the nature of $\mathcal{D}_{\text{DMD}}^-$ cannot be defined a priori.

While the multi-layer analysis was originally designed for CNNs, we extend it to transformer-based DNNs by omitting the initial dimensionality-reduction step and focusing solely on the embedding activations that is associated with classification.

Feature Squeezing: FS [23] assumes that the perturbation introduced by AAs can be effectively removed by image pre-processing techniques, computing a score based on the distance between the model’s output for the original image and its pre-processed versions.

We consider the three filters proposed on [23], namely: Bit Reduction, which uniformly quantizes values by discarding their least-significant bits; Median Filter, a standard filter for noise removal based on the median operator; and Non Local Mean Filter (NLM), a weighted denoising that averages pixels whose surrounding patches are similar. While the former is defined by the number of bits used to quantize the original input, the median filter depends on the filter’s kernel size. NLM pre-processing is determined by parameters such as the search window size, the patch size for similarity computation, and the Gaussian filter bandwidth controlling the smoothing.

We highlight that FS is originally designed for AA detection, and its efficiency depends on selecting filters tailored for the attacks to be detected. Moreover, the approach is model-agnostic as the selected filters are created without using information about the DNN under analysis.

III. PROPOSED METHOD

We deal with DNNs classifier accepting input images encoded as tensors \mathbf{X} and outputting one of L possible labels $\ell(\mathbf{X}) = l$ with $l \in \{0, \dots, L-1\}$. We assume that this happens through the computation of an intermediate vector $\mathbf{z}(\mathbf{X}) \in \mathbb{P}^L$ of positive numbers whose sum is normalized to 1 that estimates the match between \mathbf{X} and each possible label, so that $\ell(\mathbf{X}) = \arg \max \mathbf{z}(\mathbf{X})$.

The entries of $\mathbf{z}(\mathbf{X})$ provide information about how sharp the network’s final decision is: a vector dominated by a single large entry, with all other components negligible, indicates that the network assigns overwhelming confidence to the chosen label; by contrast, a vector with several entries close to the maximum suggests that alternative labels are regarded as nearly as plausible as the output one.

The model is composed of a sequence of intermediate layers with arbitrarily shaped inputs \mathbf{x} and outputs \mathbf{y} , referred to as activations. We assume the availability of datasets composed of input-label pairs, divided into *training* set $\mathcal{D}^{\text{train}}$, *validation* set \mathcal{D}^{val} , generally used for tuning, and *test* set $\mathcal{D}^{\text{test}}$, used for performance evaluation, whose cardinalities are denoted by $|\cdot|$. For instance, the number of input-label pairs in the training set is $|\mathcal{D}^{\text{train}}|$, and the set is represented as¹ $\{\mathbf{X}_t, l_t\}_{t=0}^{|\mathcal{D}^{\text{train}}|-1}$.

The main idea of the proposed framework is to compute a score that captures the coherence between patterns of intermediate activations and the network’s output, as visualized in Figure 1. The activation processing, described in detail in Section III-A, is performed on a set of target layers, and

¹The index t is used to enumerate instances within any of the aforementioned sets. When omitted, it refers to a generic element of the set; when used without a specified range, it is assumed to span the entire set.

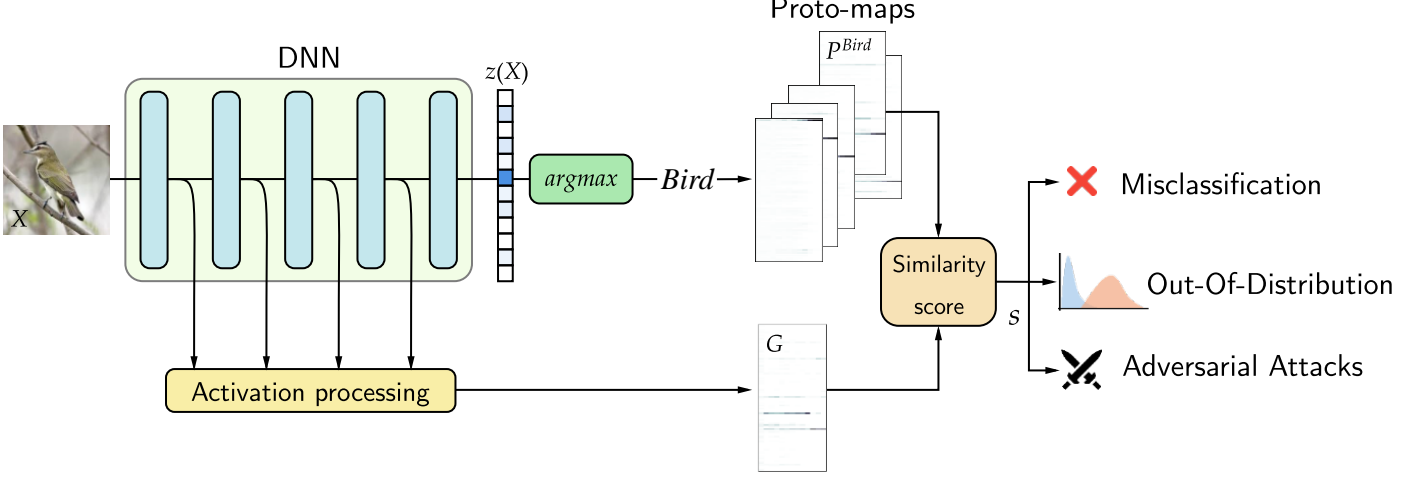


Fig. 1: MACS’s overview. The intermediate activations are processed, leading to a compact representation of the model’s decision process (G), which is compared with typical values for the predicted class (P) resulting in a confidence score (s) that can be used for detecting misclassified samples, OOD inputs or AAs.

consists of: *i*) a dimensionality reduction step transforms high-dimensional activations into low-dimensional ones, namely corevectors, capturing and compressing the layer’s parameters for efficient downstream processing while minimizing information loss; *ii*) a clustering step identifies patterns within the corevectors space; *iii*) an empirical association step relating the identified clusters with the classification labels, creating a vector that estimates the classification probabilities ($z(X)$) from the features encoded in a single layer. By gathering these estimates from the set of target layers, we create the proposed classification-map (G), which maps the decision process throughout the DNN’s layers and is compared against typical values for the predicted class (P) to compute the proposed confidence score (s), as described in detail in Section III-B.

A. Internal Activation Processing

As analyzing raw intermediate activations is computationally prohibitive, the first processing step is computing a low-dimensional vector that captures the information flowing through a layer. We focus on layers accepting an input $x \in \mathbb{R}^n$ and producing an output $y \in \mathbb{R}^m$ via the affine transformation:

$$y = [\mathbf{W} | \mathbf{b}] \begin{bmatrix} x \\ 1 \end{bmatrix} = \mathbf{A} \begin{bmatrix} x \\ 1 \end{bmatrix}, \quad (1)$$

where $\mathbf{W} \in \mathbb{R}^{m \times n}$ and $\mathbf{b} \in \mathbb{R}^m$ contain weights and biases, and $\mathbf{A} \in \mathbb{R}^{m \times (n+1)}$ is the overall affine operator. Note that eq. (1) is general and applies to layers expressible through parameter rearrangements, e.g., the isomorphic unrollings of convolutional layers [28] or Vision Transformers (ViT) [29] ones. Non-linear activation functions, normalization, or aggregation steps are considered as separate layers here.

A reduced representation of x is obtained by projecting it onto a κ -dimensional subspace of \mathbb{R}^{n+1} through a column-orthonormal matrix $\mathbf{B} \in \mathbb{R}^{(n+1) \times \kappa}$, i.e.,

$$\mathbf{v} = \mathbf{B}^\top \begin{bmatrix} x \\ 1 \end{bmatrix}.$$

The vector \mathbf{v} , hereinafter referred to as corevector, approximates the original output activations if an alternative transformation $\mathbf{A}' \in \mathbb{R}^{m \times \kappa}$ yields approximate outputs, i.e., minimizing

$$\left\| \mathbf{A}'\mathbf{v} - \mathbf{A} \begin{bmatrix} x \\ 1 \end{bmatrix} \right\|^2 = \left\| \mathbf{A}'\mathbf{B}^\top \begin{bmatrix} x \\ 1 \end{bmatrix} - \mathbf{A} \begin{bmatrix} x \\ 1 \end{bmatrix} \right\|^2,$$

where $\|\cdot\|$ is the classical square vector norm.

Averaging over random, zero-mean, and unit-variance inputs reduces this to minimizing $\|\mathbf{A}'\mathbf{B}^\top - \mathbf{A}\|_F^2$, where $\|\cdot\|_F$ is the Frobenius norm. The optimal solution is obtained from the SVD of \mathbf{A} :

$$\mathbf{A} = \mathbf{P}\Sigma\mathbf{Q}^\top,$$

with \mathbf{P} and \mathbf{Q} orthonormal and Σ containing non-increasing singular values. Let $\mathbf{Q}' \in \mathbb{R}^{(n+1) \times \kappa}$ and $\Sigma' \in \mathbb{R}^{m \times \kappa}$ denote the matrices formed by the first κ columns of \mathbf{Q} and Σ , respectively. From the SVD properties, $\mathbf{B} = \mathbf{Q}'$ and $\mathbf{A}' = \mathbf{P}\Sigma'$, making the corevectors to be computed as:

$$\mathbf{v} = \mathbf{Q}'^\top \begin{bmatrix} x \\ 1 \end{bmatrix} \quad (2)$$

The second step aims to statistically capture patterns within the corevectors’ space through unsupervised clustering, allowing their distinction from unseen ones, e.g., ones generated by OOD or AA samples.

As best practice, all corevectors are normalized according to mean and variance obtained from $\mathcal{D}^{\text{train}}$, after which they are clustered using a Gaussian Mixture Model (GMM) [30], which

defines a map from corevectors into a membership vector $\mathbf{m} \in \mathbb{P}^C$ with components:

$$m_i = \frac{\gamma_i(\mathbf{v})}{\sum_{j=0}^{C-1} \gamma_j(\mathbf{v})} ; i \in \{0, \dots, C-1\}, \quad (3)$$

where

$$\gamma_i(\mathbf{v}) = \frac{\phi_i}{\sqrt{(2\pi)^\kappa \det(\mathbf{K}_i)}} e^{-\frac{1}{2}(\mathbf{v} - \boldsymbol{\mu}_i)^\top \mathbf{K}_i^{-1}(\mathbf{v} - \boldsymbol{\mu}_i)},$$

with $\boldsymbol{\mu}_i \in \mathbb{R}^\kappa$ being cluster center, $\mathbf{K}_i \in \mathbb{R}^{\kappa \times \kappa}$ the covariance matrix, and ϕ_i is the membership probability.

Although we focus on GMM, we highlight that any clustering algorithm can be adopted, providing the definition of membership functions $\gamma_i : \mathbb{R}^\kappa \mapsto \mathbb{R}^+$ that yield increasing values the more likely \mathbf{v} is to belong to the i -th cluster.

The third step consists of associating clustering assignments, i.e., LLF in the compressed activation space, with human-understandable HLF represented by the labels of each instance. As in [22], this relationship is modeled assuming two functions, $\varsigma : \mathbb{R}^\kappa \mapsto \{0, \dots, C-1\}$ and $\tau : \mathbb{R}^\kappa \mapsto \{0, \dots, L-1\}$, that associate corevectors to clusters and labels, respectively, with a probabilistic link between them expressed as:

$$\Pr\{\tau(\mathbf{v}) = l\} = \sum_{i=0}^{C-1} \Pr\{\tau(\mathbf{v}) = l | \varsigma(\mathbf{v}) = i\} \Pr\{\varsigma(\mathbf{v}) = i\}, \quad (4)$$

with $l = 0, \dots, L-1$. In eq. (4) we may interpret the membership vector \mathbf{m} in terms of probabilities to set $\Pr\{\varsigma(\mathbf{v}) = i\} = m_i$, while the matrix $\mathbf{U}_{l,i} = \Pr\{\tau(\mathbf{v}) = l | \varsigma(\mathbf{v}) = i\}$ needs to be estimated from data.

By considering inputs, labels and associated corevectors as $\{\mathbf{X}_t, l_t, \mathbf{v}_t\}_{t=0}^{|\mathcal{D}^{\text{train}}|-1}$, the number joint events $u_{l,i}$ can be computed as:

$$u_{l,i} = |\{\tau(\mathbf{v}_t) = l \wedge \varsigma(\mathbf{v}_t) = i\}|,$$

and each element of \mathbf{U} , $\mathbf{U}_{l,i}$, can be estimated as:

$$\mathbf{U}_{l,i} = \frac{u_{l,i}}{\sum_{j=0}^{L-1} u_{j,i}}.$$

Once estimated, \mathbf{U} can be used to compute the vector $\mathbf{g} = \mathbf{U}\mathbf{m}$ which acts as a network output estimation. In other words, $\mathbf{g} \in \mathbb{P}^L$ estimates the probability of a sample belonging to each class (label) computed from the LLF within the respective layer's activations.

Note that the corevectors dimension κ and number of clusters C are the only two hyper-parameters controlling the \mathbf{g} extraction, influencing the clustering and, consequently, the capability of \mathbf{g} to act as an estimator of $\ell(\mathbf{X})$.

B. Classification Maps and Scoring Function

As illustrated in Figure 1, the three-stage processing chain is attached to a selected set of target affine layers. The extracted vectors \mathbf{g}_j are arranged as column-wise into the matrix $\mathbf{G} = [\mathbf{g}_j]_{j=0}^{M-1} \in \mathbb{R}^{L \times M}$, referred to as the classification-map, where M denotes the number of layers from which a \mathbf{g}_j is extracted. Note that it may be

desirable to process activations of every affine layer; however, a trade-off between computational cost and retrieved information relevance suggests focusing on a subset of layers. The classification-maps can be visualized as an image representing the internal signature of the network's decision process.

In the final step, we create a scoring function that estimates the model's confidence during inference by quantifying how well \mathbf{G} matches with reference classification-maps from training samples, hereafter denoted as proto-maps, hence capturing typical decision processes well encoded within the model.

Consider the classification-maps $\{\mathbf{G}_t\}_{t=0}^{|\mathcal{D}^{\text{train}}|-1}$. The proto-map \mathbf{P}^l for each class $l \in \{0, \dots, L-1\}$ accumulates information from classification-maps of correctly classified samples with high-confidence, i.e., samples well fitted within the model, formally described by the set $\mathcal{P}^l = \{\mathbf{G}_t | \ell(\mathbf{X}_t) = l_t \wedge \max(\mathbf{z}(\mathbf{X}_t)) > \delta\}$, with δ being an user-defined threshold for the model's confidence.

The proto-map for each possible label \mathbf{P}^l is computed by the accumulation:

$$\overline{\mathbf{P}}^l = \sum_{t \in \mathcal{P}^l} \mathbf{G}_t,$$

followed by a normalization across the labels direction, such that each column of \mathbf{P}^l is an element of \mathbb{P}^L .

Note that the proposed proto-maps are similar to the "signature values" in the CAM analysis done in [21] w.r.t. the set conditions in \mathcal{P}^l , differing as the former encodes typical decision process values for each label, while the latter directly encodes the high-dimensional intermediate activations.

Finally, the score of a sample is computed as the cosine similarity between its classification-map and the proto-map of its predicted label, as:

$$s_t = \frac{\mathbf{P}^{\ell(\mathbf{X}_t)} \odot \mathbf{G}_t}{\|\mathbf{P}^{\ell(\mathbf{X}_t)}\|_F \|\mathbf{G}_t\|_F}, \quad (5)$$

where \odot is the element-wise product. Note that $s \in [0, 1]$ since $\mathbf{P}^{\ell(\mathbf{X}_t)}$ and \mathbf{G}_t contain only non-negative values.

As a final remark, we highlight that the SVD decomposition to compute \mathbf{Q}' , corevectors clustering, \mathbf{U} matrix, and proto-maps \mathbf{P} are computed offline, only once over $\mathcal{D}^{\text{train}}$, making the computation of s at inference time a relatively lightweight process.

IV. EXPERIMENTAL SETUP

This section briefly describes the experimental setup used in this paper².

Our experiments consider the well-known CIFAR-100 [31] dataset, containing images of $L = 100$ fine-grained classes. To evaluate performance under distributional shifts, we use CIFAR-100C [32], which is obtained from CIFAR-100's $\mathcal{D}^{\text{test}}$ by applying 13 corruptions with 5 intensity levels. For OOD detection, we consider Places365 [33] and SVHN [34],

²Source code available at: <https://github.com/SSIGPRO/Peepholes-Analysis>

standard benchmarks semantically distant from CIFAR-100’s distribution [35].

The driving examples are the classical image classifiers from the Visual Geometry Group (VGG) [36] and ViT [29] families. Specifically, we use VGG16, a 16-layer CNN and ViTB16, a 12-transformer layer with 16×16 patches. VGG16 is characterized by its sequential arrangement of convolutional layers, followed by fully connected ones for the final classification. ViTB16 is an encoder-only transformer architecture characterized by 12 encoders, each composed of a multi-head attention layer followed by a sequence of two fully connected layers. Both models are implemented within the TorchVision[37] library from PyTorch[38]. Since the models are pre-trained on the ImageNet classification task, we replace the final fully connected layer with a new layer containing L output units. The resulting architectures are then fine-tuned on the CIFAR-100 $\mathcal{D}^{\text{train}}$.

Classification performance is quantified by the top-1 accuracy, i.e., the ratio between the number correctly classified and the total samples. VGG16 and ViTB16 reach accuracies of 77.00% and 86.64%, respectively, on CIFAR-100’s $\mathcal{D}^{\text{test}}$. For VGG16 we extended the internal activation analysis to 13 out 16 layers composing the neural network, excluding only the initial three convolutional layers. For ViTB16, we select both fully connected layers immediately after the attention mechanism of each encoder block and the final classification head, resulting in a total of 25 analyzed layers.

For each of these target layers, κ and C are tuned to maximize the top-3 accuracy computed by comparing the position of the 3 highest entries in \mathbf{g}_t and the true label l_t .

A. Adversarial Attacks

To evaluate AA detection, we select four established attack algorithms in literature: Basic Iterative Method (BIM) [39], Projected Gradient Descent (PGD) [40], Carlini & Wagner (CW) [41], and DeepFool (DF) [42]. We use CW’s original implementation provided by the authors [41] and the TorchAttacks library [43] implementations for the other AAs. All attacks are untargeted, and the attack budget, ϵ , is set at $8/255$. The generation of adversarial samples relies on different distance metrics: the Euclidean norm is used for CW and DF, whereas PGD and BIM minimize the Chebyshev norm. Table I reports the Attack Success Rate (ASR) for each model and attack under test, which corresponds to the ratio between the amount of adversarial samples generated from correctly classified samples that successfully mislead the DNN and the total amount of correctly classified samples.

TABLE I: ASR (\uparrow) for the proposed attacks over VGG16 and ViTB16.

AA	VGG16	ViTB16
BIM	0.84	0.68
CW	1.00	1.00
DF	0.82	0.53
PGD	0.95	0.89

V. NUMERICAL EVIDENCE

This section evaluates MACS regarding its ability to improve the confidence of classifications, and to detect OOD and AA images by comparing it against the SOTA baselines: MSP [6], DOC [2], Rel-U [3], FS [23], and DMD [4] in its three variants: DMD-b, DMD-a, and DMD-u. To contextualize this comparison, Table II summarizes the reference approaches and the applications they were designed to address.

As discussed in Section II-D, DOC and Rel-U are not designed for AA detection, nor FS and DMD for confidence estimation; however, these approaches are applicable and tested for these applications, highlighting their shortcomings and MACS’s flexibility.

Note that all approaches ultimately compute a confidence score, which we normalize between $[0, 1]$, with 1 meaning that the prediction should be trusted and 0 that it should not be trusted. As such, a low score suggests that the sample should not be trusted, i.e., it is OOD, generated by an AA, or an incorrectly classified in-distribution sample.

To quantitatively assess the performance of the considered methods in the various scenarios, we compute Area Under the Reciever Operating Curve (AUC) [44] and FPR^* . The former measures overall discrimination capability by evaluating performance across all possible confidence-score thresholds. In contrast, FPR^* is obtained by selecting a threshold such that 95% of correctly classified in-distribution samples have their scores above it, this reflects a practical acceptance/rejection criterion when deciding whether to trust a prediction.

TABLE II: Proposed and SOTA approaches applications. ✓ indicates that the method is designed for the task. ○ indicates that the method was not designed for the task, but was included for comparison.

Method	Confidence	OOD	Attack Detection
MACS (our)	✓	✓	✓
Rel-U [3]	✓	✓	○
DOC [2]	✓	✓	○
DMD [4]	○	✓	✓
FS [23]	○	○	✓

A. proto-maps

Computing s as in (5) by matching the proto-map \mathbf{P} associated to the DNN prediction with the classification-map \mathbf{G} obtained at inference time yields two principal advantages. First, it enables a more refined assessment of the validity of the predicted label by leveraging internal network activations, without incurring the additional computational cost associated with back-propagation-based procedures, as in DMD. Second, s captures the statistical structure of the decision-making process across the entire network, rather than relying on a single layer or solely on the softmax output. Consequently, the proposed framework yields an unsupervised reliability estimate of the DNN’s predictions, thereby obviating the need for example OOD or AA samples for integrating multi-layer information, as required by DMD-a or DMD-u.

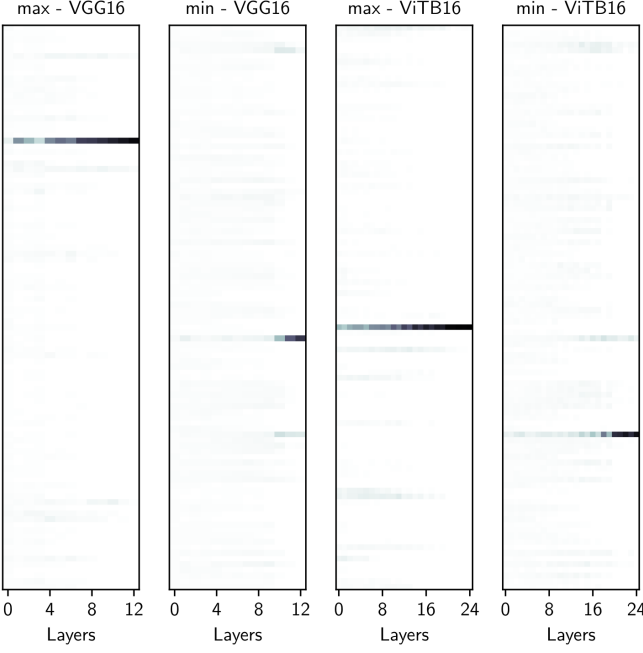


Fig. 2: Examples of \mathbf{P} computed from VGG16 and ViTB16. For each network, we display the proto-maps with the largest and smallest Frobenius norm. Columns correspond to the indices of the analyzed layers, while rows represent the dataset classes.

Figure 2 illustrates examples of \mathbf{P} computed from VGG16 and ViTB16. For each DNN we selected \mathbf{P} that have the maximum and minimum Frobenius norm. Each \mathbf{P} captures the characteristic decision-making trajectory of the reference DNN for correctly classified samples with high confidence belonging to a specific class. Note that each class induces a characteristic activation pattern, and the proposed score quantifies how much the \mathbf{G} deviates from that class-specific pattern. Importantly, its performance is not biased by the prevalence of the predicted class across the layers of \mathbf{P} .

B. Scoring in-Distribution Inputs

In this initial evaluation, the confidence scores produced by all methods listed in Table II are employed to determine, in a straightforward manner, whether predictions are correct or incorrect.

Note that, in this application, DMD-a's regressor is trained on all wrongly classified samples, i.e., $\mathcal{D}_{\text{DMD}}^- = \{\mathbf{X}_t \in \mathcal{D}^{\text{train}} \mid \ell(\mathbf{X}_t) \neq l_t\}$, and an equally populated subset of the correctly classified samples, $\mathcal{D}_{\text{DMD}}^+ = \{\mathbf{X}_t \in \text{shuffle}(\mathcal{D}^{\text{train}}) \mid \ell(\mathbf{X}_t) = l_t\}_{t=0}^{|\mathcal{D}_{\text{DMD}}^-|}$.

Figure 3 shows the score distributions conditioned by correct and incorrect classifications³. The profiles related to MACS evidence how the proposed score in (5) exhibits less overconfidence than the other metrics, as s rarely approaches a value of 1. This property allows incorrectly classified samples to be pushed toward low-confidence regions of the distribution.

³KDE approximation of the distributions.

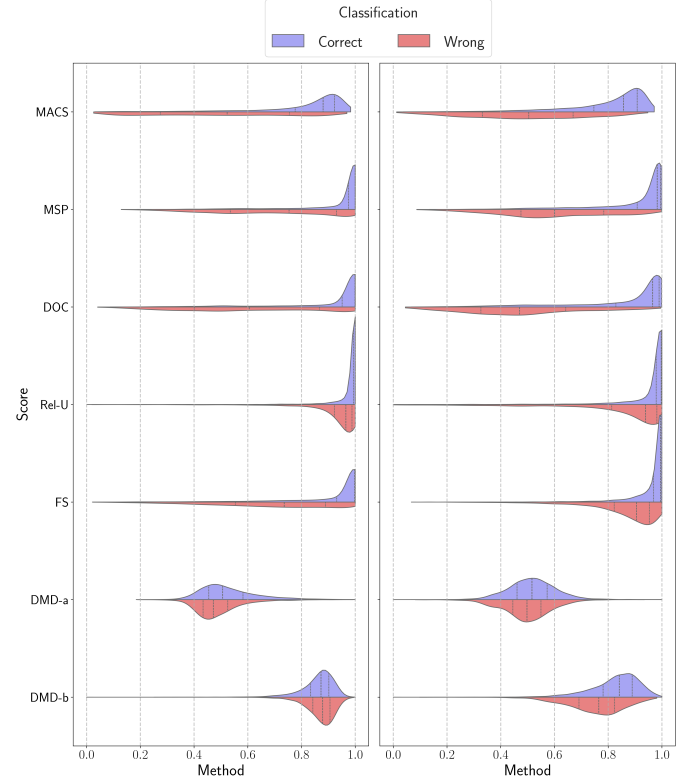


Fig. 3: Confidence scores distribution for correctly and misclassified samples over VGG16 (left) and ViTB16 (right).

TABLE III: AUC (\uparrow) and FPR* (\downarrow) values for the proposed and reference methods over VGG16 and ViTB16.

Method	VGG16		ViTB16	
	FPR*	AUC	FPR*	AUC
MACS	0.63	0.83	0.55	0.87
MSP	0.65	0.87	0.57	0.90
DOC	0.64	0.87	0.58	0.90
Rel-U	0.80	0.85	0.78	0.82
FS	0.76	0.85	0.75	0.86
DMD-b	0.97	0.46	0.83	0.72
DMD-a	0.92	0.61	0.90	0.56

However, this advantage comes at the cost of assigning lower confidence scores to a portion of correctly classified samples, compared with the alternative methods.

To quantitatively evaluate the distributions in Figure 3, Table III reports the AUCs and FPR*’s, showing that MSP achieves the best AUCs. These results confirm that the model itself is a very good estimator, whereas the other methods provide only surrogate approximations of its predictive certainty. Interestingly, among the methods not originally designed for this task, DMD performs poorly in both single-layer DMD-b and multi-layer DMD-a versions, and FS reaches good AUCs, but its high FPR*’s indicate the shortcomings in generalizing the method to this task. Regarding the other methods, DOC achieves the highest AUCs, and MACS the lowest FPR* in both cases, which is favorable in a practical scenario since it is more important to attribute a lower score for low-confidence samples than a high score for high-confidence ones.

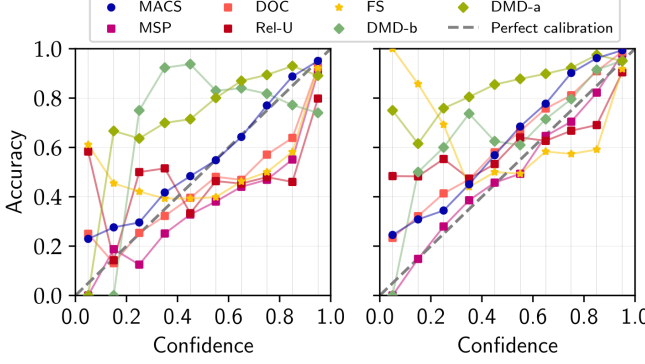


Fig. 4: Reliability diagrams for VGG16 (left) and ViTB16 (right).

The results in Figure 3 are tied to the scores’ calibration, which evaluates the average accuracy of samples as a function of their scores, typically visualized as a reliability diagram, that bins samples by score and measures their average accuracy. A perfectly calibrated score is a diagonal line, and a score below or above this line is over- or under-confident, respectively. The corresponding diagrams for CIFAR-100 are shown in Figure 4. Consistent with the conditional distributions in Figure 3, the scores produced by MACS exhibit under-confidence.

Interestingly, MACS has accuracy that monotonically increases with the confidence for both cases, while the reference methods have undesirable jumps caused by the accuracy’s high-variability under the limited number of samples with low confidence, ultimately demonstrating that the DOC, Rel-U, and FS are not well calibrated. In fact, even MSP shows these problems for ViTB16, even though a good calibration for this model was expected according to [7].

C. Out-Of-Distribution Detection

This section evaluates how well the scores allow for differentiating ID samples, i.e., typical images seen by the model during its training, from OOD ones, i.e., substantially different images which are not well encoded within the DNN’s parameters.

First, we consider the detection of corrupted samples using the CIFAR-100C dataset. Note that DMD is hard-limited to its aware mode (DMD-a), meaning that corrupted samples (from CIFAR-100C’s \mathcal{D}^{val}) are used as supervision to fit its regressor, hence being interpreted here as an upper-bound for unsupervised methods.

Figure 5 shows the AUC for each corruption intensity for samples from CIFAR-100 and CIFAR-100C’s $\mathcal{D}^{\text{test}}$. Note that MSP is over-confident for both types of samples, meaning that a high score is attributed to either case, regardless of the corruption intensity, making it a non-robust score for this task, as demonstrated by the results from [45]. DMD-a consistently yields good AUCs, which is expected since it is the only supervised method. Regarding MACS, results show that it outperforms all other non-supervised methods for ViTB16, while reaching the same level of performance as DMD-a on

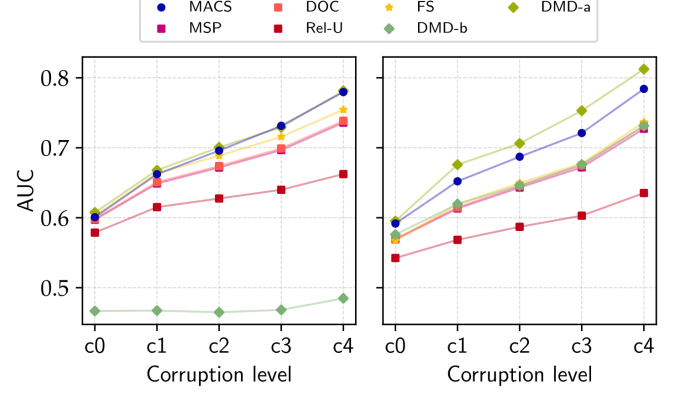


Fig. 5: AUC progression with the corruption intensity using ID samples from CIFAR-100’s $\mathcal{D}^{\text{test}}$ and corrupted samples from CIFAR-100C, with cX indicating the corruption intensity, for VGG16 (left) and ViTB16 (right). As the intensity increases, scores decrease, making it easier to differentiate normal from corrupted samples.

VGG16. It is worth noting that FS, a method not designed for this task, outperforms DOC and Rel-U, even though its performance is below the proposed method on the modern model ViTB16.

Next, we evaluate an OOD scenario using SVHN and Places365. In this case, DMD-u is set by training the regressor with samples from the other dataset, i.e., $\mathcal{D}_{\text{DMD}}^- = \mathcal{D}_{\text{Places365}}^{\text{val}}$ for testing SVHN and $\mathcal{D}_{\text{DMD}}^- = \mathcal{D}_{\text{SVHN}}^{\text{val}}$ for testing Places365. In turn, DMD-a is set by fitting its regressor on $\mathcal{D}_{\text{DMD}}^-$ using samples from the same dataset as it is tested on; i.e., $\mathcal{D}_{\text{DMD}}^- = \mathcal{D}_{\text{SVHN}}^{\text{val}}$ and $\mathcal{D}_{\text{DMD}}^- = \mathcal{D}_{\text{Places365}}^{\text{val}}$ for testing SVHN and Places365, respectively. As such, DMD-a is considered as an upper-bound, while DMD-u is a realistic scenario where the distribution shift’s nature cannot be anticipated.

Table IV summarizes the results, showing that DMD-a consistently yields the best AUCs for Places365, but its performance greatly degrades for its DMD-u version, demonstrating how the dataset used to fit the regressor impacts its detection capabilities. As originally observed in [4], DMD’s performance for convolutional models benefits from analyzing multiple layers (low performance on DMD-b), while the improvement is marginal for transformer-based models, hardly justifying the required overhead. Among the unsupervised methods, MACS and FS consistently achieve the best performance, being comparable with each other.

D. Attack Analysis

For the final application, we evaluate how effectively s identifies AA samples by reporting the corresponding AUCs in comparison to the reference methods. Regarding sample selection, as in [23], we only consider attacked samples for images correctly classified by the model, and that had their predicted label successfully changed by the attack. For DMD-a, the regressor is trained with samples from the attack used for testing, i.e., $\mathcal{D}_{\text{DMD}}^- = \mathcal{D}_X^{\text{val}}$ for testing each AA $X \in \{\text{BIM}, \text{CW}, \text{DF}, \text{PGD}\}$. In turn DMD-u’s regressor is

TABLE IV: OOD Detection performance in terms of AUC for VGG16 and ViTB16. ID samples correspond to CIFAR-100.

Method	VGG16		ViTB16	
	Places365	SVHN	Places365	SVHN
MACS	0.85	0.81	0.88	0.90
MSP	0.84	0.82	0.84	0.90
DOC	0.84	0.82	0.85	0.91
Rel-U	0.74	0.64	0.67	0.67
FS	0.80	0.86	0.86	0.94
DMD-b	0.69	0.45	0.97	0.90
DMD-a	0.99	0.88	0.99	0.95
DMD-u	0.99	0.82	0.03	0.51

trained using samples from all other AAs, i.e., $\mathcal{D}_{\text{DMD}}^- = \{\mathcal{D}_Y^{\text{val}} \forall Y \in \{\text{BIM}, \text{CW}, \text{DF}, \text{PGD}\} \mid Y \neq X\}$ for testing each AA X , being a more realistic case since the AA being tested is unknown.

The achieved results are reported in Table V. CW and DF, due to hyper-parameter choice, modify z such that the incorrect label attains only a slightly higher probability than the correct one, leading to low-confidence misclassification. In contrast, BIM and PGD push the model toward wrong predictions with high confidence. It is straightforward to deduce that scores based solely on $z(\mathbf{X})$ (i.e., MSP, DOC, and Rel-U) will be effective at detecting CW and DF as these attacks naturally produce low MSP values; however, their detection capability drops drastically under attacks like BIM and PGD, which deliberately induce high-confidence errors, thereby compromising these confidence-based detectors by design. As such, we argue that methods which analyze the intermediate activations (i.e., DMD and MACS) are more robust to AAs by design. MACS's score is low in both cases given that \mathbf{G} greatly mismatches the prediction's \mathbf{P} . Since MACS takes into consideration also the last layer of the reference models, our results are influenced by it. However, the dependency over multiple layers allows MACS to be more robust to BIM and PGD with respect to MSP, DOC and Rel-U.

DMD-a and DMD-u achieve high AUCs for DF and PGD, and low scores for BIM and CW. Note that the pairs of attacks for which DMD has high and low scores do not correspond to the separation of attacks based on their effects on the MSP, indicating that it is caused by the dataset dependency for training its regressor, reinforcing the idea that such a dependency can become a shortcoming of the method.

Different from the OOD case, DMD shows significant improvements in its multi-layer version for both VGG16 and ViTB16, corroborating to the idea that methods which analyze the internal activations are inherently more robust to AAs.

As expected, FS outperforms other methods in this task, especially on VGG16, while MACS is a valid alternative among the unsupervised methods. On ViTB16, MACS outperforms FS on three attacks out of four.

E. Unknown Input Conditions

Up to this point, the different cases under investigation have been analyzed separately. However, in a practical scenario, it is impossible to know in advance whether inputs are ID, OOD, or AA, making an approach robust for all three cases desirable.

TABLE V: Attack Detection performance in terms of AUC under different attacks on VGG16 and ViTB16.

Method	VGG16				ViTB16			
	BIM	CW	DF	PGD	BIM	CW	DF	PGD
MACS	0.78	0.90	0.93	0.79	0.85	0.95	0.95	0.87
MSP	0.51	0.96	0.96	0.50	0.56	0.95	0.93	0.55
DOC	0.52	0.94	0.96	0.50	0.56	0.93	0.92	0.55
Rel-U	0.47	0.90	0.86	0.47	0.48	0.80	0.73	0.50
FS	0.89	0.97	0.89	0.91	0.83	0.97	0.91	0.81
DMD-b	0.42	0.47	0.57	0.56	0.75	0.74	0.87	0.80
DMD-a	0.78	0.65	0.94	0.92	0.86	0.60	0.98	0.98
DMD-u	0.70	0.54	0.87	0.90	0.83	0.57	0.97	0.98

To test this scenario, we compute a single threshold from ID samples as shown in Section V-B, reflecting the impossibility of anticipating distribution shifts in OOD or the typology AA samples. Regarding DMD-a, this evaluation exposes the shortcomings of being a supervised approach, requiring its regressor to be trained to distinguish correctly from incorrectly classified ID samples.

Accordingly, Tables VIa and VIb report the FPR* for VGG16 and ViTB16, respectively. Each column refers to a possible application and we highlight in bold the best-performing method and underline the second-best. MACS consistently ranks among the best-performing methods across all scenarios, thereby providing the most favorable overall trade-off.

F. Computation Complexity and Time

To summarize this aspect, Table VII shows the average computation time overhead rescaled by the average inference time for each method, considering only their online steps on an NVIDIA H100 device with 80GB of RAM. Regarding MACS's inference overhead, the dimensionality reduction step, a.k.a, computing eq. (2), corresponds to roughly 90% and 60% of the overhead for VGG16 and ViTB16, respectively, which is caused by the higher activation sizes of convolutional layers.

Another advantage of MACS is its low online computational cost. All expensive operations, namely the layers' parameter SVD decomposition (\mathbf{Q}'), clustering of the training-set corevectors (\mathbf{v}), and the empirical association between LLF, HLF, and the proto-maps (\mathbf{U} , \mathbf{P}), are performed once offline. At inference time, MACS requires only lightweight matrix multiplications and a cosine similarity over compact representations.

In contrast, DMD requires a back-propagation step for each evaluated sample, leading to a substantially higher and model-dependent computational burden. This difference is especially evident in DMD-b, whose best configuration according to our tests uses backpropagation for VGG16, but does not use it for ViTB16. Note that DMD-a and DMD-u differ only in the datasets used for training their regressors, so their computational overhead is the same.

DOC and Rel-U, due to hyperparameter settings incur minimal overhead. FS remains the most expensive method due to its NLM filtering.

TABLE VI: FPR^* (\downarrow) given the threshold computed for ID analysis. $mean^*$ is the mean of all FPR^* 's including the ID case, and $mean$ excludes the ID FPR^* . **Bold** and underline indicate the lowest and second lowest FPR^* 's, respectively.

(a) VGG16

ID	Corruption					OOD		Attacks				mean	max	
	c0	c1	c2	c3	c4	SVHN	Places365	BIM	CW	DF	PGD			
MACS	0.63	0.79	0.73	0.67	0.62	0.54	0.46	0.44	0.77	0.50	0.36	0.73	0.60	0.79
MSP	0.65	<u>0.81</u>	0.76	0.74	<u>0.71</u>	0.68	0.57	0.50	0.82	<u>0.30</u>	0.19	0.85	<u>0.63</u>	0.85
DOC	<u>0.64</u>	0.79	<u>0.74</u>	<u>0.71</u>	0.68	<u>0.65</u>	0.53	<u>0.45</u>	0.81	0.58	<u>0.22</u>	0.84	<u>0.63</u>	<u>0.84</u>
Rel-U	0.80	0.90	0.90	0.90	0.91	0.91	0.98	0.90	0.98	0.68	0.85	0.99	0.89	0.99
FS	0.76	0.84	0.79	0.77	0.74	0.70	<u>0.47</u>	0.67	0.28	0.16	0.67	0.32	0.60	0.84
DMD-b	0.97	0.97	0.97	0.98	0.97	0.98	1.00	0.89	0.98	0.96	0.96	0.96	0.96	0.98
DMD-a	0.92	0.90	0.82	0.76	0.73	0.67	0.75	0.83	0.95	0.95	0.84	0.85	0.83	0.95

(b) ViTB16

ID	Corruption					OOD		Attacks				mean	max	
	c0	c1	c2	c3	c4	SVHN	Places365	BIM	CW	DF	PGD			
MACS	0.55	0.81	0.75	0.71	0.66	0.57	0.34	0.40	0.51	0.30	0.23	0.53	0.53	0.81
MSP	<u>0.57</u>	<u>0.84</u>	0.79	0.75	0.71	0.65	0.34	0.49	0.69	<u>0.30</u>	<u>0.30</u>	0.71	0.60	0.84
DOC	0.58	<u>0.84</u>	<u>0.78</u>	<u>0.74</u>	<u>0.70</u>	<u>0.63</u>	<u>0.28</u>	0.45	0.67	0.60	0.39	0.70	0.62	<u>0.84</u>
Rel-U	0.78	0.92	0.92	0.92	0.92	0.93	1.00	0.95	0.98	0.85	0.92	0.98	0.94	0.98
FS	0.75	0.88	0.85	0.82	0.80	0.73	0.20	0.51	0.37	0.16	0.43	0.48	<u>0.57</u>	0.88
DMD-b	0.83	0.90	0.88	0.86	0.83	0.78	0.55	0.11	0.64	0.82	0.54	0.61	0.68	0.90
DMD-a	0.90	0.94	0.93	0.92	0.91	0.89	0.70	0.96	0.95	0.94	0.93	0.92	0.91	0.96

TABLE VII: Average computation time overhead per sample normalized according to the average model inference time.

Method	VGG16	ViTB16
MACS	2.82 ± 0.6	$(9.5 \pm 0.3) \times 10^{-1}$
DOC	$(1.8 \pm 0.1) \times 10^{-4}$	$(1.1 \pm 0.8) \times 10^{-4}$
Rel-U	$(4.1 \pm 0.3) \times 10^{-3}$	$(1.6 \pm 0.2) \times 10^{-3}$
FS	$(2.9 \pm 0.3) \times 10^2$	$(1.8 \pm 0.6) \times 10^2$
DMD	$(2.5 \pm 0.2) \times 10^1$	$(4.7 \pm 0.6) \times 10^1$
DMD-b	1.2 ± 0.3	$(6.1 \pm 0.3) \times 10^{-2}$

Table VII summarizes the average online overhead of each method, normalized by their respective inference times on an NVIDIA H100 (80 GB RAM). For MACS, the dimensionality-reduction step (eq. (2)) dominates the cost, accounting for approximately 90% of the overhead on VGG16 and 60% on ViTB16, reflecting the larger activation sizes of convolutional layers.

VI. CONCLUSIONS

This work introduced MACS, a post-hoc method for estimating prediction confidence in generic pre-trained DNNs by analyzing their internal activations. The resulting score enables confidence estimation, OOD detection, and AA detection within a unified and lightweight framework. MACS incorporates dimensionality reduction for scalability, unsupervised clustering to identify activation-level features, and an empirical association step linking these features to semantic labels.

We evaluated the method on VGG16, ViTB16, and the CIFAR-100, CIFAR-100C, SVHN, and Places365 datasets, comparing it against DOC, Rel-U, and the intermediate-activation method DMD. Beyond matching or outperforming these baselines in individual tasks, MACS provides consis-

tently reliable behavior across all scenarios without requiring task-specific supervision.

The results reveal a key distinction: while output-based approaches excel when errors coincide with low softmax confidence, they fail under high-confidence AAs or OOD shifts. In contrast, activation-based methods capture deviations in the internal decision process, enabling more robust detection even when the output layer is misleading. MACS exploits this advantage while avoiding the supervised regressor required by prior techniques.

Future directions include extending the framework to non-vision domains, exploring adaptive clustering strategies, and integrating MACS into training-time feedback loops to enhance calibration and robustness.

REFERENCES

- [1] “Regulation (eu) 2024/1689 of the european parliament and of the council – artificial intelligence act,” Official Journal of the European Union, OJ L 2024/1689, 12 July 2024, 2024, accessed via EUR-Lex. [Online]. Available: <https://eur-lex.europa.eu/eli/reg/2024/1689/oj>
- [2] F. Granese, M. Romanelli, D. Gorla, C. Palamidessi, and P. Piantanida, “DOCTOR: A Simple Method for Detecting Misclassification Errors,” in *Proceedings*, ser. Proceedings, Virtual event, United States, 2021, pp. 5669–5681. [Online]. Available: https://proceedings.neurips.cc/paper_files/paper/2021/file/2cb6b10338a7fc4117a80da24b582060-Paper.pdf
- [3] E. Dadalto, M. Romanelli, G. Pichler, and P. Piantanida, “A Data-Driven Measure of Relative Uncertainty for Misclassification Detection,” 2024. [Online]. Available: <https://arxiv.org/abs/2306.01710>
- [4] K. Lee, K. Lee, H. Lee, and J. Shin, “A simple unified framework for detecting out-of-distribution samples and adversarial attacks,” in *Proceedings of the 32nd International Conference on Neural Information Processing Systems*, ser. NIPS’18. Red Hook, NY, USA: Curran Associates Inc., 2018, p. 7167–7177. [Online]. Available: https://proceedings.neurips.cc/paper_files/paper/2018/file/abdeb6f575ac5c6676b747bca8d09cc2-Paper.pdf
- [5] N. Papernot and P. McDaniel, “Deep k-Nearest Neighbors: Towards Confident, Interpretable and Robust Deep Learning,” 2018. [Online]. Available: <https://arxiv.org/abs/1803.04765>

[6] D. Hendrycks and K. Gimpel, "A Baseline for Detecting Misclassified and Out-of-Distribution Examples in Neural Networks," 2018. [Online]. Available: <https://arxiv.org/abs/1610.02136>

[7] M. Minderer, J. Djolonga, R. Romijnders, F. Hubis, X. Zhai, N. Houlsby, D. Tran, and M. Lucic, "Revisiting the calibration of modern neural networks," in *Proceedings of the 35th International Conference on Neural Information Processing Systems*, ser. NIPS '21. Red Hook, NY, USA: Curran Associates Inc., 2021, pp. 15\,682–15\,694. [Online]. Available: https://proceedings.neurips.cc/paper_files/paper/2021/file/8420d359404024567b5aefda1231af24-Paper.pdf

[8] C. Guo, G. Pleiss, Y. Sun, and K. Q. Weinberger, "On calibration of modern neural networks," in *Proceedings of the 34th International Conference on Machine Learning - Volume 70*, ser. Proceedings of Machine Learning Research, D. Precup and Y. W. Teh, Eds., vol. 70. PMLR, 06–11 Aug 2017, pp. 1321–1330. [Online]. Available: <https://proceedings.mlr.press/v70/guo17a.html>

[9] A. Perez-Lebel, M. L. Morvan, and G. Varoquaux, "Beyond calibration: estimating the grouping loss of modern neural networks," in *ICLR Proceedings*, Kigali, Rwanda, May 2023. [Online]. Available: <https://hal.science/hal-03829870>

[10] A. Singh, A. Bay, B. Sengupta, and A. Mirabile, "On the dark side of calibration for modern neural networks," 2021. [Online]. Available: <https://www.gatsby.ucl.ac.uk/~balaji/udl2021/accepted-papers/UDL2021-paper-074.pdf>

[11] D.-B. Wang, L. Feng, and M.-L. Zhang, "Rethinking calibration of deep neural networks: do not be afraid of overconfidence," in *Proceedings of the 35th International Conference on Neural Information Processing Systems*, ser. NIPS '21. Red Hook, NY, USA: Curran Associates Inc., 2021, pp. 11\,809–11\,820. [Online]. Available: https://proceedings.neurips.cc/paper_files/paper/2021/file/61f3a6dbc9120ea78ef75544826c814e-Paper.pdf

[12] S. A. Balanya, J. Marofas, and D. Ramos, "Adaptive temperature scaling for Robust calibration of deep neural networks," *Neural Comput. Appl.*, vol. 36, no. 14, p. 8073–8095, Feb. 2024. [Online]. Available: <https://doi.org/10.1007/s00521-024-09505-4>

[13] L. Clarté, B. Loureiro, F. Krzakala, and L. Zdeborová, "Expectation consistency for calibration of neural networks," in *Proceedings of the Thirty-Ninth Conference on Uncertainty in Artificial Intelligence*, ser. Proceedings of Machine Learning Research, R. J. Evans and I. Shpitser, Eds., vol. 216. PMLR, 31 Jul–04 Aug 2023, pp. 443–453. [Online]. Available: <https://proceedings.mlr.press/v216/clarte23a.html>

[14] C. K. I. Williams and C. E. Rasmussen, "Gaussian Processes for Regression," in *Advances in Neural Information Processing Systems*, Denver, United States, Nov. 1995. [Online]. Available: <https://hal.science/hal-03953027>

[15] Y. Gal and Z. Ghahramani, "Dropout as a Bayesian Approximation: Representing Model Uncertainty in Deep Learning," in *Proceedings of The 33rd International Conference on Machine Learning*, ser. Proceedings of Machine Learning Research, M. F. Balcan and K. Q. Weinberger, Eds., vol. 48. New York, New York, USA: PMLR, 20–22 Jun 2016, pp. 1050–1059. [Online]. Available: <http://proceedings.mlr.press/v48/gal16.pdf>

[16] C. Wei, S. Kakade, and T. Ma, "The Implicit and Explicit Regularization Effects of Dropout," in *Proceedings of the 37th International Conference on Machine Learning*, ser. Proceedings of Machine Learning Research, H. D. III and A. Singh, Eds., vol. 119. PMLR, 13–18 Jul 2020, pp. 10\,181–10\,192. [Online]. Available: <http://proceedings.mlr.press/v119/wei20d/wei20d.pdf>

[17] J. Liu, Z. Lin, S. Padhy, D. Tran, T. Bedrax Weiss, and B. Lakshminarayanan, "Simple and Principled Uncertainty Estimation with Deterministic Deep Learning via Distance Awareness," in *Proceedings of the 34th International Conference on Neural Information Processing Systems*, H. Larochelle, M. Ranzato, R. Hadsell, M. Balcan, and H. Lin, Eds., vol. 33. Curran Associates, Inc., 2020, pp. 7498–7512. [Online]. Available: https://proceedings.neurips.cc/paper_files/paper/2020/file/543e83748234f7cbab21aa0ade66565f-Paper.pdf

[18] J. Postels, M. Segù, T. Sun, L. D. Sieber, L. Van Gool, F. Yu, and F. Tombari, "On the Practicality of Deterministic Epistemic Uncertainty," in *Proceedings of the 39th International Conference on Machine Learning*, ser. Proceedings of Machine Learning Research, K. Chaudhuri, S. Jegelka, L. Song, C. Szepesvari, G. Niu, and S. Sabato, Eds., vol. 162. PMLR, 17–23 Jul 2022, pp. 17\,870–17\,909. [Online]. Available: <https://proceedings.mlr.press/v162/postels22a.html>

[19] S. Fort, J. Ren, and B. Lakshminarayanan, "Exploring the limits of out-of-distribution detection," in *Proceedings of the 35th International Conference on Neural Information Processing Systems*, ser. NIPS '21. Red Hook, NY, USA: Curran Associates Inc., 2021. [Online]. Available: https://proceedings.neurips.cc/paper_files/paper/2021/file/3941c4358616274ac2436eacf67fae05-Paper.pdf

[20] Y. Geifman and R. El-Yaniv, "Selective classification for deep neural networks," in *Proceedings of the 31st International Conference on Neural Information Processing Systems*, ser. NIPS'17. Red Hook, NY, USA: Curran Associates Inc., 2017, p. 4885–4894. [Online]. Available: https://proceedings.neurips.cc/paper_files/paper/2017/file/4a8423d5e91fda00bb7e46540e2b0cf1-Paper.pdf

[21] G. Rossolini, A. Biondi, and G. Buttazzo, "Increasing the Confidence of Deep Neural Networks by Coverage Analysis," *IEEE Transactions on Software Engineering*, vol. 49, no. 2, pp. 802–815, 2023.

[22] Y. han Liu and S. O. Arik, "Explaining Deep Neural Networks using Unsupervised Clustering," 2020. [Online]. Available: <https://arxiv.org/abs/2007.07477>

[23] W. Xu, D. Evans, and Y. Qi, "Feature Squeezing: Detecting Adversarial Examples in Deep Neural Networks," in *Proceedings 2018 Network and Distributed System Security Symposium*. Internet Society, 2018.

[24] B. Liang, H. Li, M. Su, X. Li, W. Shi, and X. Wang, "Detecting Adversarial Image Examples in Deep Neural Networks with Adaptive Noise Reduction," *IEEE Transactions on Dependable and Secure Computing*, vol. 18, no. 1, pp. 72–85, 2021.

[25] S. Jha, S. Raj, S. Fernandes, S. K. Jha, S. Jha, B. Jalaian, G. Verma, and A. Swami, "Attribution-Based Confidence Metric For Deep Neural Networks," in *Proceedings of the 33rd International Conference on Neural Information Processing Systems*, H. Wallach, H. Larochelle, A. Beygelzimer, F. d'Alché-Buc, E. Fox, and R. Garnett, Eds., vol. 32. Curran Associates, Inc., 2019. [Online]. Available: https://proceedings.neurips.cc/paper_files/paper/2019/file/bc1ad6e8f86c42a371aff945535baebb-Paper.pdf

[26] W. He, J. Wei, X. Chen, N. Carlini, and D. Song, "Adversarial example defenses: ensembles of weak defenses are not strong," in *Proceedings of the 11th USENIX Conference on Offensive Technologies*, ser. WOOT'17. USA: USENIX Association, 2017, p. 15. [Online]. Available: <https://www.usenix.org/conference/woot17/workshop-program/presentation/he>

[27] J. H. Metzen, T. Genewein, V. Fischer, and B. Bischoff, "On Detecting Adversarial Perturbations," 2017. [Online]. Available: <https://arxiv.org/abs/1702.04267>

[28] B. Praggastis, D. Brown, C. O. Marrero, E. Purvine, M. Shapiro, and B. Wang, "The svd of convolutional weights: A cnn interpretability framework," 2022. [Online]. Available: <https://arxiv.org/abs/2208.06894>

[29] A. Dosovitskiy *et al.*, "An Image is Worth 16x16 Words: Transformers for Image Recognition at Scale," 2021. [Online]. Available: <https://arxiv.org/abs/2010.11929>

[30] A. P. Dempster, N. M. Laird, and D. B. Rubin, "Maximum Likelihood from Incomplete Data Via the EM Algorithm," *Journal of the Royal Statistical Society: Series B (Methodological)*, vol. 39, no. 1, pp. 1–22, 12 2018.

[31] A. Krizhevsky and G. Hinton, "Learning multiple layers of features from tiny images," University of Toronto, Toronto, Ontario, Tech. Rep. 0, 2009. [Online]. Available: <https://www.cs.utoronto.ca/~kriz/learning-features-2009-TR.pdf>

[32] D. Hendrycks and T. Dietterich, "Benchmarking Neural Network Robustness to Common Corruptions and Perturbations," 2019. [Online]. Available: <https://arxiv.org/abs/1903.12261>

[33] B. Zhou, A. Lapedriza, A. Khosla, A. Oliva, and A. Torralba, "Places: A 10 Million Image Database for Scene Recognition," *IEEE Transactions on Pattern Analysis and Machine Intelligence*, vol. 40, no. 6, pp. 1452–1464, 2018.

[34] Y. Netzer, T. Wang, A. Coates, A. Bissacco, B. Wu, A. Y. Ng *et al.*, "Reading digits in natural images with unsupervised feature learning," in *NIPS workshop on deep learning and unsupervised feature learning*, vol. 2011, no. 5. Granada, 2011, p. 7. [Online]. Available: http://ufldl.stanford.edu/housenumbers/nips2011_housenumbers.pdf

[35] J. Yang, K. Zhou, and Z. Liu, "Full-Spectrum Out-of-Distribution Detection," *Int. J. Comput. Vision*, vol. 131, no. 10, p. 2607–2622, Jun. 2023.

[36] K. Simonyan and A. Zisserman, "Very Deep Convolutional Networks for Large-Scale Image Recognition," 2015. [Online]. Available: <https://arxiv.org/abs/1409.1556>

[37] S. Marcel and Y. Rodriguez, "Torchvision the machine-vision package of torch," in *Proceedings of the 18th ACM International Conference on Multimedia*, ser. MM '10. New York, NY, USA: Association for Computing Machinery, 2010, p. 1485–1488.

[38] J. Ansel *et al.*, "PyTorch 2: Faster Machine Learning Through Dynamic Python Bytecode Transformation and Graph Compilation," in *Proceedings of the 29th ACM International Conference on Architectural Support for Programming Languages and Operating Systems*, Volume 2,

ser. ASPLOS '24. New York, NY, USA: Association for Computing Machinery, 2024, p. 929–947.

[39] A. Kurakin, I. J. Goodfellow, and S. Bengio, “Adversarial examples in the physical world,” in *Artificial intelligence safety and security*. Chapman and Hall/CRC, 2018, pp. 99–112.

[40] A. Madry, A. Makelov, L. Schmidt, D. Tsipras, and A. Vladu, “Towards deep learning models resistant to adversarial attacks,” 2019. [Online]. Available: <https://arxiv.org/abs/1706.06083>

[41] N. Carlini and D. Wagner, “Towards Evaluating the Robustness of Neural Networks,” in *2017 IEEE Symposium on Security and Privacy (SP)*. Los Alamitos, CA, USA: IEEE Computer Society, May 2017, pp. 39–57.

[42] S.-M. Moosavi-Dezfooli, A. Fawzi, and P. Frossard, “DeepFool: A Simple and Accurate Method to Fool Deep Neural Networks,” in *2016 IEEE Conference on Computer Vision and Pattern Recognition (CVPR)*, 2016, pp. 2574–2582.

[43] H. Kim, “Torchattacks: A PyTorch Repository for Adversarial Attacks,” 2021. [Online]. Available: <https://arxiv.org/abs/2010.01950>

[44] T. Fawcett, “An introduction to roc analysis,” *Pattern Recognition Letters*, vol. 27, no. 8, pp. 861–874, 2006, rOC Analysis in Pattern Recognition.

[45] S. Liang, Y. Li, and R. Srikant, “Enhancing The Reliability of Out-of-distribution Image Detection in Neural Networks,” 2020. [Online]. Available: <https://arxiv.org/abs/1706.02690>



Lorenzo Capelli He received his B.Sc. (with Honors) in biomedical engineering in 2021 and his M.Sc. (with Honors) in electronic engineering from the University of Bologna in 2024. He is currently pursuing a Ph.D. in Engineering and Information Technology for Structural and Environmental Monitoring and Risk Management within the Statistical Signal Processing Group. His research focuses on signal processing, explainable AI, and model trustworthiness.



Leandro de Souza Rosa has a BSc (2013) in Computer Engineering and obtained a Ph.D. in 2019 from the Institute of Mathematics and Computer Sciences at The University of São Paulo, Brazil, which was partially developed at the Department of Electrical and Electronic Engineering, Imperial College London, U.K. He worked as a postdoc researcher at the Istituto Italiano di Tecnologia (Genova, Italy), in the Faculty of Mechanical, Maritime and Materials Engineering, Delft University of Technology (Delft, Netherlands), and La Sapienza University of Rome (Rome, Italy). He currently holds a researcher position in the Department of Electrical, Electronic and Information Engineering of the University of Bologna (Bologna, Italy). His research interests include hardware design, perception, robotics, and machine learning, focusing on interactions between humans and autonomous systems.



Gianluca Setti is the Dean of the Computer, Electrical, Mathematical Sciences and Engineering Division and a Professor of Electrical and Computer Engineering at KAUST. Before moving to KAUST, he was with the University of Ferrara (1997-2017) and with Politecnico di Torino (2017-2022) as a Professor of Electronics, Signal and Data Processing. He held also several positions as Visiting Professor/Scientist at EPFL (2002, 2005), UCSD (2004), IBM (2004, 2007) and at University of Washington (2008, 2010). He served as the Editor-in-Chief for

the IEEE Transactions on Circuits and Systems - Part II (2006-2007) and of the IEEE Transactions on Circuits and Systems - Part I (2008-2009). Since 2019 he is the first non-US Editor-in-Chief of the Proceedings of the IEEE, the flagship journal of the IEEE. In 2010, he served as IEEE CAS Society President. In 2013-2014 he was the first non North-American Vice President of the IEEE for Publication Services and Products. Dr. Setti received several awards, including the 2004 IEEE CAS Society Darlington Award, 2013 IEEE CAS Society Meritorious Service Award, 2013 IEEE CAS Society Guillemain-Cauer Award, and the 2019 IEEE Transactions on Circuits and Systems Best Paper Award. Since 2016, he is also a Fellow of the IEEE. His research interests include recurrent neural networks, EMC, compressive sensing and statistical signal processing, biomedical circuits and systems, power electronics, IoT, circuits and systems for machine learning, and applications of AI techniques for anomaly detection and predictive maintenance.



Mauro Mangia received the B.Sc. and M.Sc. degrees in electronic engineering and the Ph.D. degree in information technology from the University of Bologna, Bologna, Italy, in 2005, 2009, and 2013, respectively. He was a Visiting Ph.D. Student at the École Polytechnique Fédérale de Lausanne in 2009 and 2012. He is currently an Associate Professor with the Department of Electrical, Electronic and Information Engineering of the University of Bologna within the Statistical Signal Processing Group. He is also a member of both the Advanced Research Center for Electronic Systems (ARCES) and the Alma Mater Research Institute for Human-centered Artificial Intelligence. He is the scientific coordinator of several international research projects funded by public agencies, including the Italian Ministry of University and Research, the Italian Space Agency (ASI), and the European Space Agency (ESA), as well as projects supported by private entities such as Rete Ferroviaria Italiana (RFI) and Thales Alenia Space. His research interests include nonlinear systems, explainable artificial intelligence, machine learning and AI, anomaly detection, Internet of Things, Big Data analytics, and optimization. He was a recipient of the 2013 IEEE CAS Society Guillemain-Cauer Award and of the 2019 IEEE BioCAS Transactions Best Paper Award. He received the Best Student Paper Award at the IEEE International Symposium on Circuits and Systems (ISCAS 2011, as student) and at the IEEE International Instrumentation and Measurement Technology Conference (I2MTC 2024, as supervisor).



Riccardo Rovatti (M'99-SM'02-F'12) received the M.S. degree in electronic engineering and the Ph.D. degree in electronics, computer science, and telecommunications from the University of Bologna, Italy, in 1992 and 1996, respectively. He is currently a Full Professor of electronics at the University of Bologna. He has authored more than 300 technical contributions to international conferences and journals and two volumes. His research focuses on mathematical and applicative aspects of statistical signal processing, on machine learning for signal processing, and on the application of statistics to nonlinear dynamical systems. He was a Distinguished Lecturer of the IEEE CAS Society for the years 2017-2018. He was a recipient of the 2004 IEEE CAS Society Darlington Award, the 2013 IEEE CAS Society Guillemain-Cauer Award, and the 2019 IEEE BioCAS Transactions Best Paper Award. He received the Best Paper Award at ECCTD 2005 and the Best Student Paper Award at the EMC Zurich 2005 and at the International Symposium On Circuits and Systems (ISCAS) 2011. He is an IEEE fellow for his contribution to nonlinear and statistical signal processing applied to electronic systems.